Drops Floating on Granular Rafts: A Tool for Liquid Transport and Delivery

Etienne Jambon-Puillet, Christophe Josserand, Suzie Protière

LANGMUIR

pubs.acs.org/Langmuir

# Drops Floating on Granular Rafts: A Tool for Liquid Transport and Delivery

Etienne Jambon-Puillet,*,†,§ Christophe Josserand,†,‡ and Suzie Protière†

†Sorbonne Université, UPMC Univ Paris 06, CNRS, UMR 7190, Institut Jean Le Rond d'Alembert, F-75005 Paris, France
‡Laboratoire d'Hydrodynamique (LadHyX), UMR7646 CNRS-Ecole Polytechnique, 91128 Palaiseau CEDEX, France

S Supporting Information

ABSTRACT: Solid particles can modify the properties of liquid interfaces and are therefore widely used to coat drops, bubbles, and stabilize emulsions and foams. Here, we propose a new, easy, and affordable method to produce millimetric to centimetric water-in-water capsules using solid particles. We prevent the coalescence of a water drop at an oil−water interface using a monolayer of large, dense, and hydrophobic particles: a "granular raft". The capsule is then formed by a mechanical instability occurring when the interface collapses under the combined load of the floating drop and particle weight. During the destabilization, the water drop sinks into the water subphase through an oil-particle film which covers it to produce the armored capsule. By modeling the raft as a heavy membrane, we predict the floating drop shape, the raft deformation, its destabilization and highlight the complex dual nature (solid- and liquid-like) of the capsule shell. Because armored capsules' content is isolated, transportable, and easily releasable, they are great candidates for applications requiring transport of water-soluble compounds in aqueous systems such as green chemistry or cell biology.
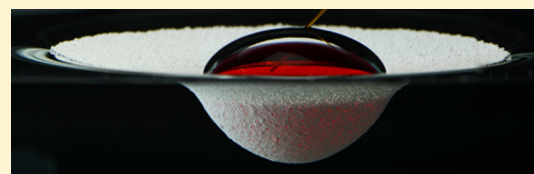
INTRODUCTION

The targeted delivery of active ingredients is of particular interest for a broad range of applications (from biomedical technologies to food and personal care). The active ingredient, for instance, a drug, needs to be shielded from the environment, transported in a capsule to a desired location, and released on demand. Today, the large development of microfluidic systems has enabled the formation of such capsules at the microscale using different techniques: for example, by using colloids,[1−3] layer by layer deposition,[4] or the polymerization of the intermediate phase of double emulsions.[5,6] These methods produce a wide range of tailored capsules but remain technical, costly, and only work at the microscale. In particular, water-in-water emulsions are currently being investigated as they have important potential applications in the food industry, for green chemistry, or in cell biology. However, they cannot be stabilized by simply using surfactants and are therefore challenging to produce.[7−9]

In parallel, another method to produce millimetric encapsulated droplets consists in coating them individually with hydrophobic particles, thus creating the so-called "liquid marbles".[10,11] Here, the liquid is protected by a rigid shell; therefore, the drop can be grabbed with tweezers and manipulated without any spillage or contamination.[10,12] By using engineered particles, liquid marbles can then be functionalized (with magnetic[13] or pH sensitive[14] particles, for example) and become miniature biochemical reactors or sensors.[15,16] Liquid marbles are very affordable and easy to produce and manipulate. However, they must be produced manually, and a drop in a miscible liquid cannot be encapsulated using this technique. To produce cheap millimetric water-in-water capsules, a method where gelatin droplets coated with hydrophobic particles are solidified, then thrown in an aqueous colloidal suspension, and finally melted was proposed.[17] However, this method is limited as it needs many different chemicals in both phases and is rather cumbersome.

Here, we propose a new strategy to easily produce inexpensive millimetric to centimetric stable water-in-water capsules. We inject water on a monolayer of large, dense, hydrophobic particles at an oil−water interface: a "granular raft".[18,19] The particles "bridge" the interface: they are partially wetted at their top and bottom by water while entrapping a thin layer of oil, thus preventing the drop coalescence and allowing the drop to float on the raft. Because the particles are heavy, the raft can then be destabilized when loading it, either by increasing the drop size or with an external trigger. It then sinks and encapsulates the floating water drop in a thin layer of oil and particles to form what we call an armored capsule (see Movies S1 and S2). The formed droplet shares many of the advantages of liquid marbles as they are cheap, easy to produce, and manipulate under water. However, using this new method enables the encapsulation of a liquid in a miscible solution, which can then be released at will. We can predict the floating drop shape and the spontaneous destabilization of the raft. We then demonstrate the potential applications of these armored capsules for liquid transport and delivery.

4437

■ EXPERIMENTAL SECTION

We fill a glass tank with deionized water (density $\rho_w = 1$ g cm^{-3}) and a thick layer (>1 cm) of light mineral oil from Sigma-Aldrich (density ρ_o = 0.838 g cm^{-3}, oil−water interfacial tension $\gamma = 46$ mN/m). We then carefully sprinkle dense particles above the interface. They get trapped at the oil−water interface and spontaneously aggregate, forming a monolayer that we call a granular raft.

We use either pigmented glass beads from Sigmund Lindner GmbH: SiO$_2$ $\rho_p = 2.5$ g cm^{-3} or zirconium oxide beads from Glen Mills Inc.: ZrO$_2$ $\rho_p = 3.8$ g cm^{-3}. They are polydisperse and not perfectly spherical but are cheap and available in large quantities. We also used high end very high density yttria-stabilized zirconium oxide beads from Glen Mills Inc.: VHD $\rho_p = 6.0$ g cm^{-3} which are monodisperse ($d = 200$ μm) and spherical (see the Supporting Information for details on the particles). Their mean diameter and oil−water contact angle vary in the range $200 < d$ (μm) < 875 and $120 < \theta_y$ (deg) < 145.

Once the raft is formed, we place a small drop at its center by injecting deionized water dyed with food coloring (Figure 1a). The
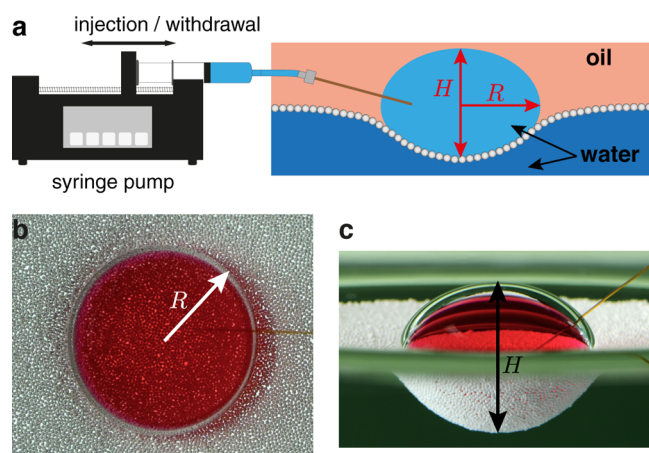
Figure 1. (a) Experimental setup. Water is injected on top of the raft with a capillary. The drop volume is controlled with a syringe pump. The drop height H and the radius R are drawn. Top (b) and side (c) picture of a typical experiment (ZrO$_2$ $d = 250$ μm). The drop radius is $R = 6.6$ mm.

drop volume is controlled with a syringe pump (PHD ULTRA from Harvard Apparatus) by pumping in or out small amounts of dyed water quasi-statically. The experiment is lit and imaged from the top and the side with two cameras (Nikon D800E, Figure 1b,c). The side camera is slightly tilted downward (angle $\lesssim 8$ deg) to see the top of the drop when it is below the water surface. The images are then analyzed using ImageJ and MATLAB.

■ RESULTS AND DISCUSSION

Figure 2 shows a typical experiment. The drop volume V is increased gradually until the interface destabilizes. The last image (Figure 2(6)) shows the droplet shape right before its destabilization. When its volume reaches $V = 11.25$ mL, the droplet sinks. The drop remains axisymmetric during the whole experiment, but its cross-sectional shape evolves as the liquid is injected. We first focus on the drop shape and record the drop radius R (measured from the top view) as well as the drop height H (Figure 1). Figure 3 shows the measurements corresponding to the drop in Figure 2. As V is increased, the drop radius first grows rapidly, the slope then decreases quickly, and the radius saturates (Figure 3a). The drop height, however, increases monotonically during a typical experiment and quickly reaches a linear dependence with the volume (Figure
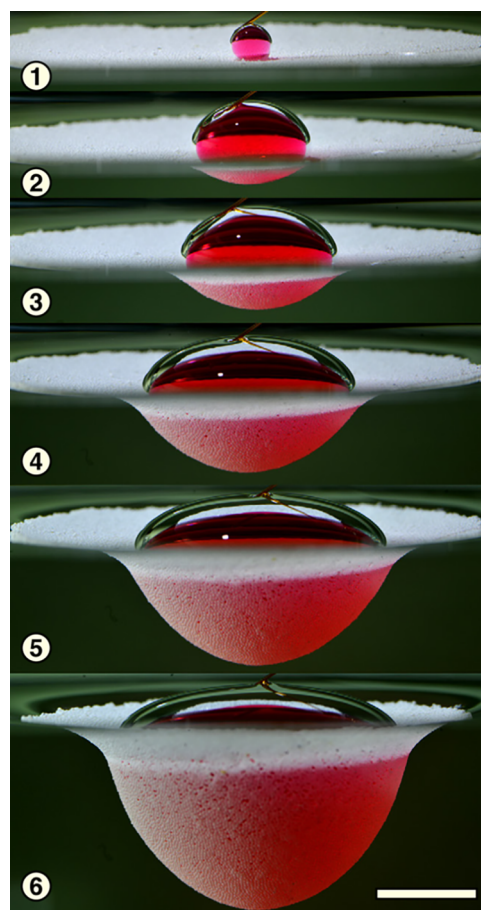
Figure 2. Drop floating on a SiO$_2$ raft ($d = 350$ μm). The drop volume increases from top to bottom: $V = 0.05, 0.7, 1.45, 3.4, 5.8,$ and 9.75 mL. Scale bar: 1 cm.

3b). In Figure 3c, we plot H as a function of R which informs us about the drop aspect ratio $H/2R$. At very low volumes, the drop is spherical (Figure 2(1)), then it takes an oblate shape (Figure 2(2,3), and Figure 3 for $5 \lesssim R$ (mm) $\lesssim 10$) which ultimately becomes more complex: the upper part of the drop and the part in contact with the raft then evolve completely differently (Figure 2(4−6)).

Because the forces acting on the drop and the raft are gravity, capillarity, and buoyancy; a natural length scale in our problem is the capillary length, $l_c = \sqrt{\gamma/(\rho_w - \rho_o)g} \approx 5.4$ mm. For drops much smaller than l_c, capillarity dominates and they stay spherical, whereas for larger drops, gravity is no longer negligible and the shape of our floating drops results from a complex interplay between the drop and raft deformation. The closest situation to what we observe is perhaps the one of a bubble trapped below the water surface[20] or equivalently a droplet sustained by a thin gas layer on a liquid bath. The latter case can be realized by vibrating the bath,[21] evaporating the drop,[22] or by using liquid marbles made with very hydrophobic powders.[23] However still, the bath interface is a pure liquid, whereas in the present case, the raft interface has a more complex structure. Here, the particles not only prevent coalescence by forming a bridged interface but also affect the drop shape through the raft deformation which depends on their size and density. This is illustrated in Figure 4d,e which shows two floating drops of the same volume on different rafts which clearly have different shapes. Figure 4a quantifies these
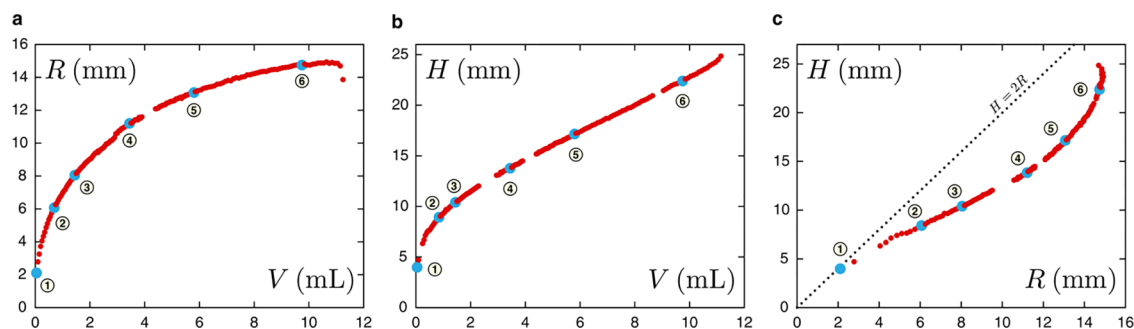
Figure 3. Shape of the drop in Figure 2 as its volume is increased. The blue data points correspond to the pictures in Figure 2. The dotted line represent a spherical shape for which $H = 2R$.
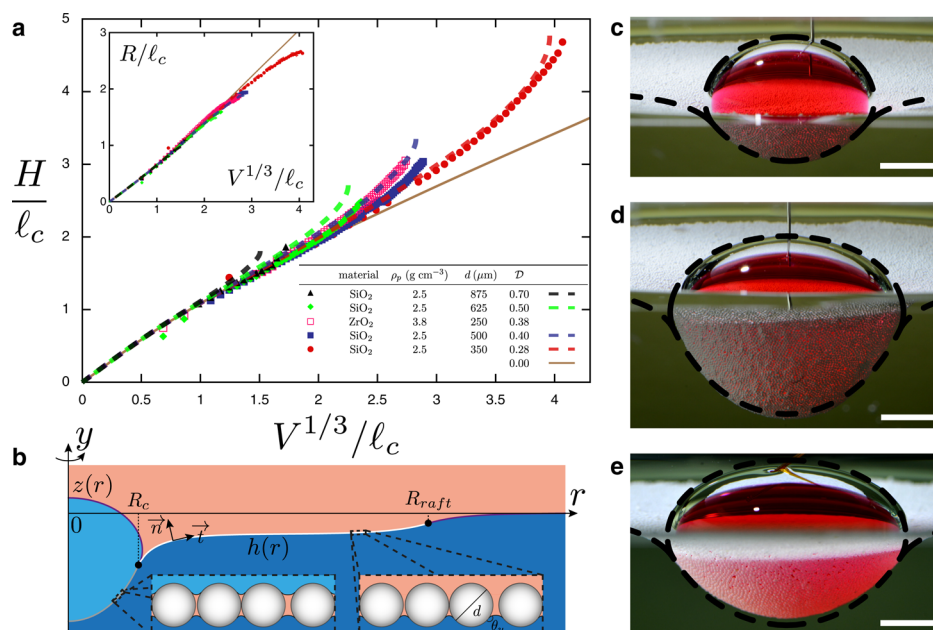

Figure 4. (a) Dimensionless drop shape (H and R) as the drop volume increases for rafts made with particles of different sizes and densities. The dashed curves are the results of the model for the same values of $\mathcal{D}$, whereas the solid curve represents the limiting case $\mathcal{D} = 0$. (b) Schematic of the model. The upper drop interface $z(r)$ and the bath interface $h(r)$ are drawn. The nature of the bath interface changes from a bridged interface for $0 < r < R_c$ to a raft for $R_c < r < R_{\text{raft}}$ and finally to a bare liquid interface for $r > R_{\text{raft}}$. (c−e) Comparison of theoretical and experimental drop profiles; scale bars: 5 mm. Drops on a ZrO$_2$ raft ($\mathcal{D} = 0.38$) of two different volumes: $V^{1/3}/l_c = 2.0$ (c) and close to the maximum volume $V^{1/3}/l_c = 2.7$ (d). (e) Drop of the same volume as (d) but on a different raft (SiO$_2$ $\mathcal{D} = 0.28$).

drop shape variations for particles of different size and density (the data are made dimensionless by rescaling lengths with l_c). For volumes much below the maximum one, the drop shape is relatively unaffected by the choice of particles, whereas there is a small influence on the radius R and a significant one on the height H close to its maximum volume. Moreover, the maximum volume itself strongly depends on the particle size and density: rafts made with smaller and less dense particles are less deformed and carry bigger drops.

Therefore, we must account for the raft mechanical properties which are still not well-understood. Modeling rafts as thin floating elastic sheets explains the propagation of surface waves[24] and their buckling under compression,[25] although not completely satisfactorily.[26] To the best of our knowledge, however, drops deforming thin floating elastic sheets have only been studied in the capillary regime,[27] and azimuthal wrinkles were observed around the drop. On the other hand, in some configurations, a simpler approach for granular rafts can be used: modeling the raft as an heavy axisymmetric membranes

with an effective tension but no bending rigidity.[28,29] Even though this method has also shown its limits, because it does not account for some elastic properties of the rafts,[29] the absence of wrinkles and compression in our experiments suggests that bending is not important here. Therefore, this simpler model is sufficient to capture the pertinent physical mechanisms.

Following the theoretical work of refs,[28,29] we thus model the raft as a continuous heavy membrane of density ρ_{eff} whose tension $T(r) + \gamma$ varies along the interface. This tension has contributions from both the liquid interface γ and the contact forces between the grains $T(r)$, whereas the density $\rho_{\text{eff}} = (2/3)\phi(\rho_p - \rho_w)$ takes into account the (immersed) particle buoyancy and voids between them through ϕ the two-dimensional packing fraction (see the Supporting Information).

The liquid surrounding the raft as well as the drop's upper surface are treated as pure liquids. The drop's lower surface being in contact with the raft forms a bridge. This region of the raft consists of two liquid interfaces with a monolayer of
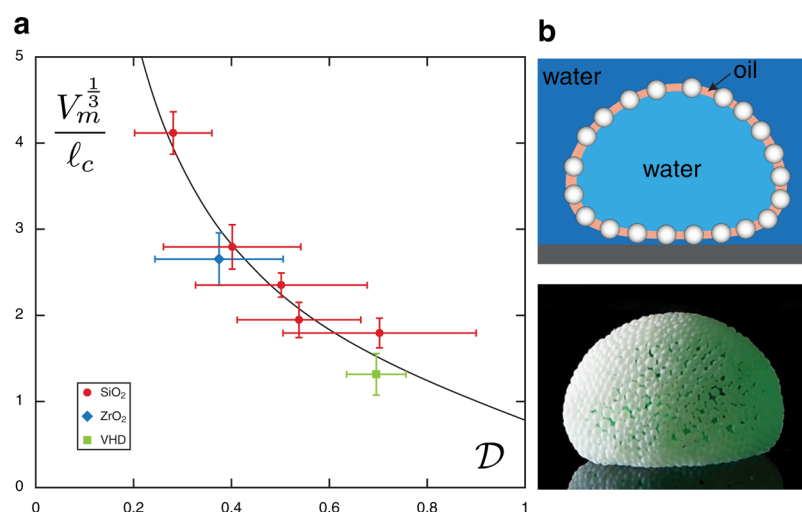
a

b

Figure 5. (a) Maximum drop volume as a function of $\mathcal{D}$ for various rafts. The black line is the theoretical prediction from the model. (b) Schematic and picture of an armored capsule (water dyed green) after a forced raft destabilization (SiO$_2$, $d = 500\ \mu m$).

particles and is modeled as one interface (similar to the rest of the raft) but with an adjusted tension $T(r) + 2\gamma$ (Figure 4b). The static equilibrium of the interfaces leads thus to the set of eqs 2 and 3 (see Theory). It results in coupled boundary value problems in each region of the space (with no free parameters) that we solve consistently numerically. We thus obtain the full drop and raft profiles, as well as the membrane tension. We can readily see from the rescaling that the particle influence can be enclosed in the dimensionless parameter

$$\mathcal{D} = \frac{\rho_{\text{eff}}}{\rho_w - \rho_o} \frac{d}{l_c} \qquad (1)$$

This parameter stands for the effective weight of the raft that is both curving the interface and varying the tension between the grains. Thus, as written, $\mathcal{D}$ compares the weight of the raft at the scale of the particles with the effect of buoyancy at the scale of the capillary length l_c. In Figure 4a, the drop shapes depend only on the parameter $\mathcal{D}$. For instance, drops on rafts made with SiO$_2$ $d = 500\ \mu m$ and ZrO$_2$ $d = 250\ \mu m$ particles behave similarly although the particles have different sizes and densities because their $\mathcal{D}$ values are similar, confirming the relevance of this parameter. As a consequence, the maximum drop volume that can be supported by the raft (also reported in Figure 5a) only depends on $\mathcal{D}$.

We compare the results of the model with the experiments in Figure 4a. The drop height H as well as its radius R as a function of the drop volume are well-reproduced for all values of $\mathcal{D}$. Figure 4c–e shows a direct comparison between pictures from a typical experiment and the result of the model. Figure 4c,d shows two drops on the same raft (same $\mathcal{D}$) but with two different volumes, whereas Figure 4d,e shows two drops of the same volume on different rafts. The complete drop shape as well as the raft shape and the position of the contact between the different interfaces are well-predicted in all cases.

This model also enables us to predict the maximum drop volume that a raft can support. In Figures 3 and 4a, the data stop at a given volume: at that maximum volume V_m, the drop sinks, destabilizes the raft, and is encapsulated to form an armored capsule (Figure 5b). In the numerics, we increase gradually the drop radius (which indirectly controls V) until we are unable to find a solution to our system of equations. In Figure 5a, we plot V_m as a function of $\mathcal{D}$. The numerical and

experimental maximum match perfectly, showing that rafts with a lower $\mathcal{D}$ carry bigger drops. Because of the simplifying assumptions used in the model (e.g., monodisperse spheres) and the experimental uncertainties, we reduce $\mathcal{D}$ by roughly 10% for polydisperse particles to obtain this very good match with the experiment. We thus took $\phi = 0.7$, about 10% lower than the expected value from random close packing (see the Supporting Information).

The limiting case $\mathcal{D} = 0$ (no particle weight) never destabilizes. This case is equivalent to pure liquid interfaces,[20] realized for bubbles trapped below water, or drops floating on a bath of the same liquid. The drop-shape deviation from this limiting case shown in Figure 4a is prominently close to the maximum volume. For $\mathcal{D} = 0$, the portion of the drop in contact with the bath is spherical, and the flat raft region below the water surface does not exist.

In Protière et al.,[29] a similar model has been used to describe the stability of granular rafts (without a drop). There, the tension decreases with the raft size and weight, and the destabilization occurs when the overall membrane tension vanishes ($T = -n\gamma$, with $n = 1$ or 2 the number of liquid interfaces, see Theory). This can be interpreted as the system having no capillary pressure to balance the raft weight. In the model presented here, the destabilization is the result of a different mechanism. Indeed, two branches of solutions are observed numerically at large volumes. Figure 6a shows the two branches on a $H = f(V)$ bifurcation diagram as well as a representative profile for each one. Figure 6b shows the tension induced by the grains at the origin $T(0)$ (where its magnitude is maximum) as the drop volume varies for both branches (the upper branch in this figure corresponds to the lower one in Figure 6a). Whatever the drop volume is, we always have $T(0) > -2\gamma$ but depending on $\mathcal{D}$, we have $-1.2 < T(0)/\gamma < -1.1$ at the maximum volume. Because the overall membrane tension $T(r) + n\gamma$ never vanishes, the origin of the destabilization is thus not straightforward. More branches might exist, and the complete bifurcation and stability analysis of the system goes beyond the scope of this article. Yet, the lower branch is the one we observe experimentally (reported in Figure 4), whereas we never see the upper one. We thus assume that the lower branch is stable whereas the upper one is unstable. The destabilization appears as the result of a saddle node bifurcation
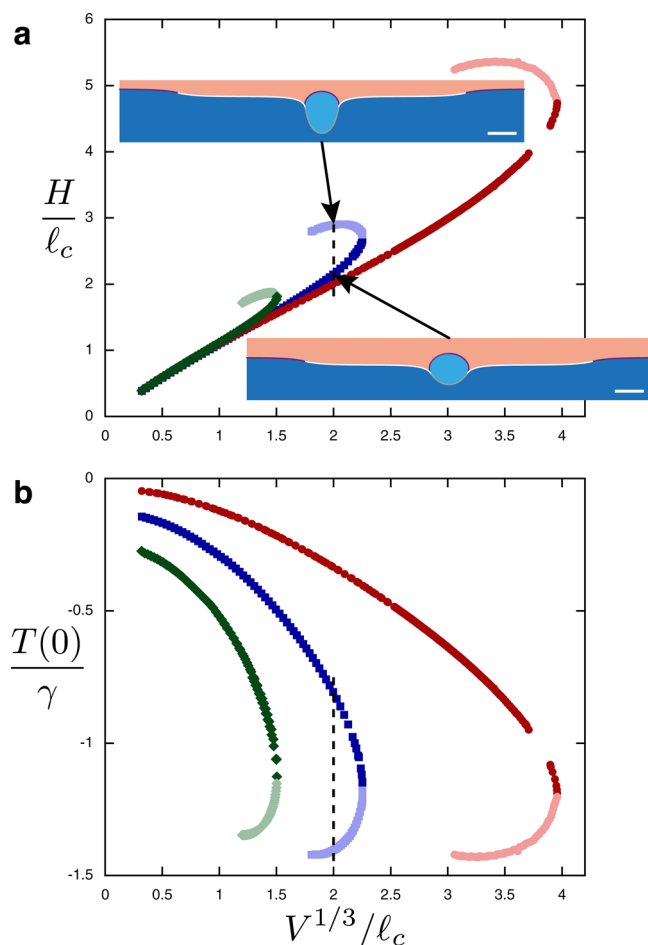
Figure 6. Full numerical results for $\mathcal{D} = 0.28$ (red circles), $\mathcal{D} = 0.50$ (blue squares), and $\mathcal{D} = 0.70$ (green diamonds). (a) Drop height as a function of its volume. (b) Minimum tension as a function of the drop volume. The first branch of the solution (assumed stable) is drawn with dark colors, whereas the second branch (assumed unstable) is drawn with lighter colors. The two numerical solutions for $\mathcal{D} = 0.50$ and $V^{1/3}/l_c = 2$ are drawn (scale bar: $2l_c$).

Figure 7. Dimensionless drop shape during successive volume increase (filled/plain) and decrease (open/dashed) for a SiO_2 raft ($d = 500$ μm). The lines and arrows are guide for the eye. The three types of drop retraction behavior are shown with side pictures.

in our system. The instability of the upper branch remains to be understood because the usual argument of vanishing surface tension does not work here (we have checked that $T(r) + n\gamma > 0$ everywhere for all of the solutions). However, it is interesting to focus on the situation near the contact line (at $r = R_c$), where the number of interfaces in the raft goes from $n = 2$ to $n = 1$. Therefore, while $T(R_c) + \gamma$ is small but positive, it varies very rapidly when entering in the domain $n = 2$ suggesting that the instability mechanisms occurs in this region. This is in agreement with the experimental observations showing that the raft breaks along R_c in contrast with the raft destabilization when no drops are present where it appears at $r = 0$.[29]

Conversely, when we start to withdraw water from an existing drop, it does not recover its previous shape. Figure 7 shows the shape of the drop (expressed as $H = f(R)$) during injection/withdrawal cycles.

Indeed, in this case, only the upper portion of the drop deforms at first: the drop radius remains constant while the height decreases. The bridged portion is pinning the contact line, thus creating adhesion between the drop and the particles in this region. Then, depending on the initial drop volume, we observe three different outcomes. If the drop is small compared
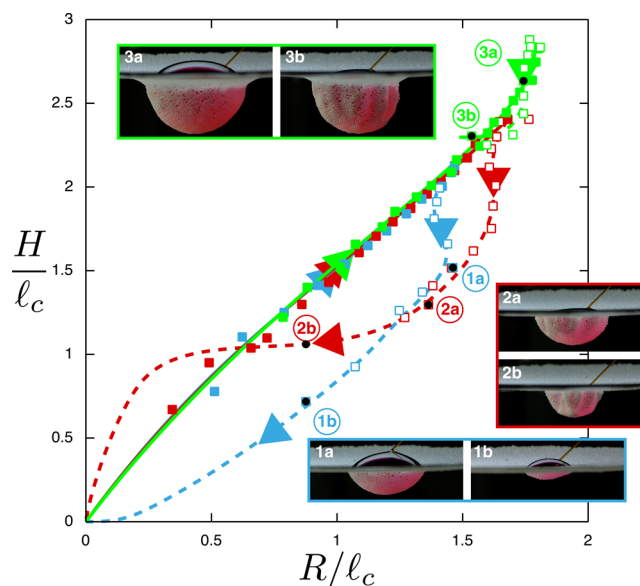
to its maximum size (Figure 7(1a,1b), $V \approx 0.45 \ V_m$), the contact line finally recedes with a stick-slip motion. The drop becomes very oblate but it can be completely removed. If the drop's initial volume is close to V_m (Figure 7(3a,3b), $V \approx 0.9$ V_m), the contact line never moves and the bridged portion of the raft starts to deform. We observe large azimuthal wrinkles, indicating that the raft is under compression in that direction and responds to it similarly to an elastic material.[26] Subsequent liquid withdrawal destabilizes the raft, and the drop either gets encapsulated or is released in the bath. At intermediate volumes (Figure 7(2a,2b), $V \approx 0.65 \ V_m$) we find a combination of the two previous behaviors, indicating a smooth transition between them. The contact line moves but the raft also deforms and wrinkles. Nonetheless, it is possible in that case to completely pump out the drop. These pumping experiments highlight the complex nature of the bridged interface, which is also the armored capsule shell. Modeling them goes beyond the scope of this article, however, we expect the adhesion of the drop to the particles[18] as well as the bending rigidity under compression of the raft[26] to be key parameters.

We finally focus on the destabilization process and the characteristics of the formed armored capsules. When the raft destabilizes, the drop sinks and drags down the raft, forming a multiphase neck that thins out and breaks (Movie S1). The majority of the initial volume gets encapsulated in what we call an armored capsule. The structure of the capsule is a single bridged interface (Figure 5b), which isolates the drop from the rest of the bath. Moreover, the particles provide some rigidity to the shell which proves useful for its manipulation. Altogether, this makes floating drops and armored capsules great candidates for various applications: they have a lot in common with liquid marbles which have been successfully used as chemical or biochemical microreactors and sensors;[16,30,31] yet, they allow to work in aqueous systems and have unique properties (see Movie S2). Indeed, the bare portion of the floating drop is accessible, allowing control and visualization of a reaction. The destabilization can be triggered, for instance, by pushing the drop downward with a stick (Figure 8a), to
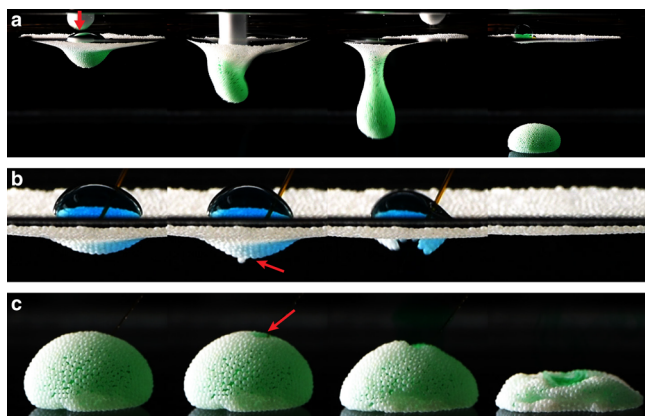
Figure 8. Image sequences extracted from Movie S2 (SiO_2 particles d = 500 μm). (a) Encapsulation is forced by pushing the drop with a Teflon stick (indicated by the red arrow). The coalescence of a floating drop (b) and opening of an armored capsule (c) are triggered by puncturing the interface with a hydrophilic needle. The red arrows indicate the position where the hole opens.

produce armored capsules of various sizes. Both the floating drop and the capsule can be transported, and their content can be released in the bath by puncturing the shell with a hydrophilic needle (Figure 8b,c).

Other methods to release or transport the capsule could be developed. For example, centrifugation could be used to destabilize the raft and thus form several capsules which can then be transported with a bulk flow. An acoustic pulse[32] or a voltage difference[33] could trigger coalescence and release the capsule's content instantly, whereas the use of an oil miscible with the active ingredient would allow a slow and controlled release through the shell. The particles used can be cheap or have various properties (magnetic or pH responsive) which widens even more the range of possibilities for controlling the capsule formation, manipulation, and release. This makes armored capsules ideal candidates for targeted delivery of active ingredients in a miscible liquid.

■ CONCLUSIONS

We have presented a new easy and affordable method to form water-in-water capsules through the destabilization of drops floating on granular rafts and studied their destabilization mechanism. A small drop deposited on top of the raft does not coalesce with the underlying water bath because the particles bridge the two interfaces, entrapping a thin protective layer of oil. Increasing the floating drop volume deforms the raft more and more until the raft destabilizes at a critical volume. It sinks with the drop and encapsulates it in an armored capsule whose shell is a thin oil-particle layer. The precise floating drop shape and raft deformation for a given volume as well as the destabilization volume depend on the raft weight through the dimensionless parameter $\mathcal{D}$, which is a scaled particle-to-fluid density ratio. By modeling the raft as a continuous heavy membrane with a varying tension, we are able to predict the drop shape, the raft deformation, and the maximum drop volume. However, if we decrease the volume of an existing droplet, the drop shape and raft deformation are not reversible. This highlights the complexity of the bridged interface which constitutes the capsule shell. Finally, we demonstrate the potential of armored capsules for liquid transport and delivery as they are easy to produce, transport, and open.

■ THEORY

We consider an axisymmetric drop at equilibrium, floating at the center of an axisymmetric raft. We use cylindrical coordinates (r, φ, y) and choose for origin $(0, 0, 0)$ the center of the drop/raft at the undeformed water level. We introduce $z(r)$ as the position of the upper drop surface which is not in contact with the raft and $h(r)$ as the position of the lower, complex interface (Figure 4b). The nature of the lower interface changes along r:

- For $0 < r < R_c$, the interface is bridged and the particles are wetted by the two water phases and the oil.
- For $R_c < r < R_{raft}$, the interface is a regular raft and the particles are wetted by the water bath and the oil.
- For $r > R_{raft}$, the interface is a regular liquid interface.

Here, R_c is the radius of contact between the drop and the raft and R_{raft} is the radius of the raft.

The shape of the upper portion of the drop $z(r)$ is given by the balance between the Laplace pressure γC and the hydrostatic pressure $-\Delta\rho g z$. Here, γ is the oil–water interfacial tension, C is the curvature of the drop surface, $\Delta\rho = \rho_w - \rho_o$ is the density difference between the oil and the water, and g is the acceleration due to gravity. Rescaling the lengths with the capillary length, $l_c = \sqrt{\gamma/\Delta\rho g}$, the equilibrium shape $z(r)$ of the drop is then defined by the relation:

$$C - C_{top} = z_{top} - z \qquad (2)$$

where C_{top} and z_{top} are the drop curvature and height at the top of the drop.

Following the work of refs,[28,29] the particle-laden interface ($h(r)$ for $r < R_{raft}$) is modeled as an effective continuous membrane of density ρ_{eff}, thickness d, and tension $T(r) + n\gamma$ at the interface between two fluids. The tension consists of two contributions: one from the liquid interface(s) $n\gamma$, where n is the number of interfaces ($n = 2$ for $r < R_c$, $n = 1$ for $r > R_c$) and one from the grains $T(r)$ that we assume independent of φ for simplicity. This membrane is subjected to its weight and bears a pressure difference ΔP, which is due to the drop and the displacement of liquids. The last portion of the interface ($h(r)$ for $r > R_{raft}$) is a regular liquid–oil interface (for which then $T(r) = 0$, $\rho_{eff} = 0$ and $n = 1$).

The equilibrium shape $h(r)$ of the particle–laden interface is given by a normal and tangential force balance. It reads in dimensionless form (rescaling lengths with $l_c = \sqrt{\gamma/\Delta\rho g}$ and tensions with γ)

$$T' - \mathcal{D}h' = 0$$

$$(T + n)\left[\frac{h''}{1 + h'^2} + \frac{h'}{r}\right] - \Delta P\sqrt{1 + h'^2} - \mathcal{D} = 0 \qquad (3)$$

where $( )' \equiv \frac{d}{dr}$ and $\mathcal{D} = \frac{\rho_{eff}}{\Delta\rho}\frac{d}{l_c}$ is the dimensionless parameter accounting for the weight of the membrane.

The effective density of the membrane $\rho_{eff} = (2/3)\phi(\rho_p - \rho_w)$ takes into account the holes in the raft with $\phi = 0.7$, the projected two-dimensional packing fraction, and the buoyancy of the particles (see the Supporting Information). Because the particles are immersed differently in the bridged and raft sections, ρ_{eff} slightly varies between them. However, the water and oil densities being similar, the difference in ρ_{eff} is small, and we neglect it for simplicity. The dimensionless pressure difference is

$$\Delta P = \begin{cases} C_{top} - z_{top} & \text{for } 0 < r < R_c \\ h(r) & \text{for } R_c < r < R_{raft} \end{cases} \quad (4)$$

For $r > R_{raft}$, we simply have

$$\left[\frac{h''}{1 + h'^2} + \frac{h'}{r} \right] - h\sqrt{1 + h'^2} = 0$$

The drop and raft equations are solved numerically using the MATLAB solver bvp5c in each region with the following boundary conditions. Axisymmetry imposes $h'(0) = z'(0) = 0$. The liquid interface relaxes at infinity: $h(\infty) = 0$. We assume the continuity of the variables h, h', z, z', and T between each regions. In particular, we have $T(R_{raft}) = 0$, that is, the contribution of the tension because of the particles vanishes at the border of the raft. We then set the values of some of the parameters by providing additional boundary conditions. The drop radius R is provided ($z'(R) = \infty$), and we assume the drop reaches the raft ($z(R_c) = h(R_c)$) with a 180° macroscopic contact angle ($z'(R_c) = h'(R_c)$). This sets C_{top}, z_{top}, and R_c. Finally, because the raft size has a little influence (as long as it is larger than the drop, see the Supporting Information), we set $R_{raft} = 10$. The control parameters are the dimensionless raft weight $\mathcal{D}$ and drop radius R, and they are varied with a continuation scheme.

The limiting case $\mathcal{D} = 0$ (neutrally buoyant particles) is equivalent to bubbles trapped below the water surface[20] or drops floating on a pool of the same liquid.[21] The interface never destabilizes, and the lower drop interface in contact with the raft becomes a portion of the sphere. The similarity with the trapped bubbles is even more striking for giant ones. Recently, Cohen et al.[34] showed that the weight of the liquid film had to be taken into account in the force balance to predict the shape of giant soap bubbles. This resulted in similar equations with the surface tension increasing along the interface (corresponding to $\mathcal{D} < 0$). Finally, there is a maximum $\mathcal{D}_{max} \approx 1.4$ in the model, which corresponds to the spontaneous destabilization of large rafts without any drop.[29]

ASSOCIATED CONTENT

Ⓢ Supporting Information

The Supporting Information is available free of charge on the ACS Publications website at DOI: 10.1021/acs.langmuir.7b04101.

Spontaneous destabilization and encapsulation of a floating drop (AVI)

Potential for liquid transport and delivery (AVI)

Details and characterization of the particles used, derivation of the raft-effective density, and effect of the raft size (PDF)

AUTHOR INFORMATION

Corresponding Author

*E-mail: e.a.m.jambonpuillet@uva.nl.

ORCID Ⓘ

Etienne Jambon-Puillet: 0000-0003-2453-0578

Present Address

§Institute of Physics, Van der Waals-Zeeman Institute, University of Amsterdam, Science Park 904, Amsterdam, The Netherlands.

REFERENCES

(1) Dinsmore, A. D.; Hsu, M. F.; Nikolaides, M. G.; Marquez, M.; Bausch, A. R.; Weitz, D. A. Colloidosomes: Selectively Permeable Capsules Composed of Colloidal Particles. *Science* **2002**, *298*, 1006−1009.

(2) Lee, D.; Weitz, D. A. Double Emulsion-Templated Nanoparticle Colloidosomes with Selective Permeability. *Adv. Mater.* **2008**, *20*, 3498−3503.

(3) Silpe, J. E.; Nunes, J. K.; Poortinga, A. T.; Stone, H. A. Generation of Antibubbles from Core−Shell Double Emulsion Templates Produced by Microfluidics. *Langmuir* **2013**, *29*, 8782−8787.

(4) Johnston, A. P. R.; Cortez, C.; Angelatos, A. S.; Caruso, F. Layer-by-layer engineered capsules and their applications. *Curr. Opin. Colloid Interface Sci.* **2006**, *11*, 203−209.

(5) Utada, A. S.; Lorenceau, E.; Link, D. R.; Kaplan, P. D.; Stone, H. A.; Weitz, D. A. Monodisperse Double Emulsions Generated from a Microcapillary Device. *Science* **2005**, *308*, 537−541.

(6) Kim, S.-H.; Kim, J. W.; Cho, J.-C.; Weitz, D. A. Double-emulsion drops with ultra-thin shells for capsule templates. *Lab Chip* **2011**, *11*, 3162−3166.

(7) Dewey, D. C.; Strulson, C. A.; Cacace, D. N.; Bevilacqua, P. C.; Keating, C. D. Bioreactor droplets from liposome-stabilized all-aqueous emulsions. *Nat. Commun.* **2014**, *5*, 4670.

(8) Vis, M.; Opdam, J.; van't Oor, I. S. J.; Soligno, G.; van Roij, R.; Tromp, R. H.; Erné, B. H. Water-in-Water Emulsions Stabilized by Nanoplates. *ACS Macro Lett.* **2015**, *4*, 965−968.

(9) Nicolai, T.; Murray, B. Particle stabilized water in water emulsions. *Food Hydrocolloids* **2017**, *68*, 157−163.

(10) Aussillous, P.; Quéré, D. Liquid marbles. *Nature* **2001**, *411*, 924−927.

(11) Aussillous, P.; Quéré, D. Properties of liquid marbles. *Proc. R. Soc. London, Ser. A* **2006**, *462*, 973−999.

(12) Kim, S.-H.; Lee, S. Y.; Yang, S.-M. Janus Microspheres for a Highly Flexible and Impregnable Water-Repelling Interface. *Angew. Chem., Int. Ed.* **2010**, *49*, 2535−2538.

(13) Zhao, Y.; Fang, J.; Wang, H.; Wang, X.; Lin, T. Magnetic Liquid Marbles: Manipulation of Liquid Droplets Using Highly Hydrophobic Fe3O4 Nanoparticles. *Adv. Mater.* **2010**, *22*, 707−710.

(14) Dupin, D.; Armes, S. P.; Fujii, S. Stimulus-Responsive Liquid Marbles. *J. Am. Chem. Soc.* **2009**, *131*, 5386−5387.

(15) McHale, G.; Newton, M. I. Liquid marbles: principles and applications. *Soft Matter* **2011**, *7*, 5473−5481.

(16) McHale, G.; Newton, M. I. Liquid marbles: topical context within soft matter and recent progress. *Soft Matter* **2015**, *11*, 2530−2546.

(17) Poortinga, A. T. Long-Lived Antibubbles: Stable Antibubbles through Pickering Stabilization. *Langmuir* **2011**, *27*, 2138−2141.

(18) Stancik, E. J.; Fuller, G. G. Connect the Drops: Using Solids as Adhesives for Liquids. *Langmuir* **2004**, *20*, 4805−4808.

(19) Horozov, T. S.; Aveyard, R.; Clint, J. H.; Neumann, B. Particle Zips: Vertical Emulsion Films with Particle Monolayers at Their Surfaces. *Langmuir* **2005**, *21*, 2330−2341.

(20) Princen, H. M. Shape of a fluid drop at a liquid-liquid interface. *J. Colloid Sci.* **1963**, *18*, 178−195.

(21) Couder, Y.; Fort, E.; Gautier, C.-H.; Boudaoud, A. From Bouncing to Floating: Noncoalescence of Drops on a Fluid Bath. *Phys. Rev. Lett.* **2005**, *94*, 177801.

(22) Maquet, L.; Sobac, B.; Darbois-Texier, B.; Duchesne, A.; Brandenbourger, M.; Rednikov, A.; Colinet, P.; Dorbolo, S. Leidenfrost drops on a heated liquid pool. *Phys. Rev. Fluids* **2016**, *1*, 053902.

(23) Ooi, C. H.; Plackowski, C.; Nguyen, A. V.; Vadivelu, R. K.; John, J. A. S.; Dao, D. V.; Nguyen, N.-T. Floating mechanism of a small liquid marble. *Sci. Rep.* **2016**, *6*, 21777.

(24) Planchette, C.; Lorenceau, E.; Biance, A.-L. Surface wave on a particle raft. *Soft Matter* **2012**, *8*, 2444−2451.

(25) Vella, D.; Aussillous, P.; Mahadevan, L. Elasticity of an interfacial particle raft. *Europhys. Lett.* **2004**, *68*, 212.

(26) Jambon-Puillet, E.; Josserand, C.; Protière, S. Wrinkles, folds, and plasticity in granular rafts. *Phys. Rev. Mater.* **2017**, *1*, 042601.

(27) Huang, J.; Juszkiewicz, M.; de Jeu, W. H.; Cerda, E.; Emrick, T.; Menon, N.; Russell, T. P. Capillary Wrinkling of Floating Thin Polymer Films. *Science* **2007**, *317*, 650−653.

(28) Abkarian, M.; Protière, S.; Aristoff, J. M.; Stone, H. A. Gravity-induced encapsulation of liquids by destabilization of granular rafts. *Nat. Commun.* **2013**, *4*, 1895.

(29) Protière, S.; Josserand, C.; Aristoff, J. M.; Stone, H. A.; Abkarian, M. Sinking a Granular Raft. *Phys. Rev. Lett.* **2017**, *118*, 108001.

(30) Xue, Y.; Wang, H.; Zhao, Y.; Dai, L.; Feng, L.; Wang, X.; Lin, T. Magnetic Liquid Marbles: A "Precise" Miniature Reactor. *Adv. Mater.* **2010**, *22*, 4814−4818.

(31) Arbatan, T.; Li, L.; Tian, J.; Shen, W. Liquid Marbles as Micro-bioreactors for Rapid Blood Typing. *Adv. Healthcare Mater.* **2012**, *1*, 80−83.

(32) McHale, G.; Elliott, S. J.; Newton, M. I.; Herbertson, D. L.; Esmer, K. Levitation-Free Vibrated Droplets: Resonant Oscillations of Liquid Marbles. *Langmuir* **2009**, *25*, 529−533.

(33) Liu, Z.; Fu, X.; Binks, B. P.; Shum, H. C. Coalescence of electrically charged liquid marbles. *Soft Matter* **2017**, *13*, 119−124.

(34) Cohen, C.; Texier, B. D.; Reyssat, E.; Snoeijer, J. H.; Quéré, D.; Clanet, C. On the shape of giant soap bubbles. *Proc. Natl. Acad. Sci. U.S.A.* **2017**, *114*, 2515−2519.